Blind restoration of retinal images degraded by space-variant blur with adaptive blur estimation

Andrés G. Marrugo[a,b], María S. Millán[a], Michal Šorel[c], and Filip Šroubek[c]

[a]Department of Optics and Optometry, Universitat Politècnica de Catalunya
Violinista Vellsolà 37, 08222 Terrassa, Spain.

[b]Facultad de Ciencias Básicas, Universidad Tecnológica de Bolívar
Km 1 vía Turbaco, Cartagena, Colombia.

[c] Institute of Information Theory and Automation, Academy of Sciences
Pod Vodárenskou věží 4, 18208 Prague 8, Czech Republic.

ABSTRACT

Retinal images are often degraded with a blur that varies across the field view. Because traditional deblurring algorithms assume the blur to be space-invariant they typically fail in the presence of space-variant blur. In this work we consider the blur to be both unknown and space-variant. To carry out the restoration, we assume that in small regions the space-variant blur can be approximated by a space-invariant point-spread function (PSF). However, instead of deblurring the image on a per-patch basis, we extend individual PSFs by linear interpolation and perform a global restoration. Because the blind estimation of local PSFs may fail we propose a strategy for the identification of valid local PSFs and perform interpolation to obtain the space-variant PSF. The method was tested on artificial and real degraded retinal images. Results show significant improvement in the visibility of subtle details like small blood vessels.

Keywords: Medical image, retinal image, deconvolution, deblurring, space-variant restoration.

1. INTRODUCTION

Blur is one of main image quality degradations in eye fundus imaging which hinders the clinical use of the images. Its main causes are: inherent optical aberrations in the eye, relative camera-eye motion, and improper focusing. Because the optics of the eye is part of the optical imaging system, eye aberrations are a common source of image degradation. To overcome this limitation, adaptive optics techniques have been successfully applied to correct the aberrations, thus producing high resolution images.[1] However, most commercial fundus cameras compensate for spherical refractive errors of the eye, but not for astigmatism[2]—let alone higher order aberrations. In general, the aberrations of the eye have a stronger impact in image degradation than the aberrations introduced by the rest of the optical system, i.e. the retinal camera (See for instance, Figure 1).

The technique for recovering an original or unblurred image from a single or a set of blurred images in the presence of a poorly determined or unknown *point spread function* (PSF) is called *blind deconvolution*. Removing blur from a single blurred image is an ill-posed problem as there are more unknowns (image and blur) than equations. Having more than one image of the same scene stabilizes solution of the problem. In retinal imaging it is not difficult to obtain a second image from the same eye, with the convenience that acquisition conditions remain quite similar. In fact, in Ref. 3 we proposed a blind deconvolution method to restore blurred retinal images acquired several months apart, even when structural changes had occurred in the retina. However, the method is limited to images blurred uniformly; in other words, we assumed the blur to be space-invariant. The space-invariant assumption is commonplace in most of the restoration methods reported in the literature,[4] but in reality it is a known fact that blur changes throughout the image.[5] In this work we consider the blur to be both unknown and space-variant (SV). This in itself is a novel and pertinent approach in retinal imaging,

Further author information: (Send correspondence to A.G. Marrugo)
A.G.M.: E-mail: agmarrugo@unitecnologica.edu.co, Telephone: +57 5 6535200 - 139.

8th Iberoamerican Optics Meeting and 11th Latin American Meeting on Optics, Lasers, and Applications,
edited by Manuel Filipe P. C. Martins Costa, Proc. of SPIE Vol. 8785, 8785D1
 · doi: 10.1117/12.2025134

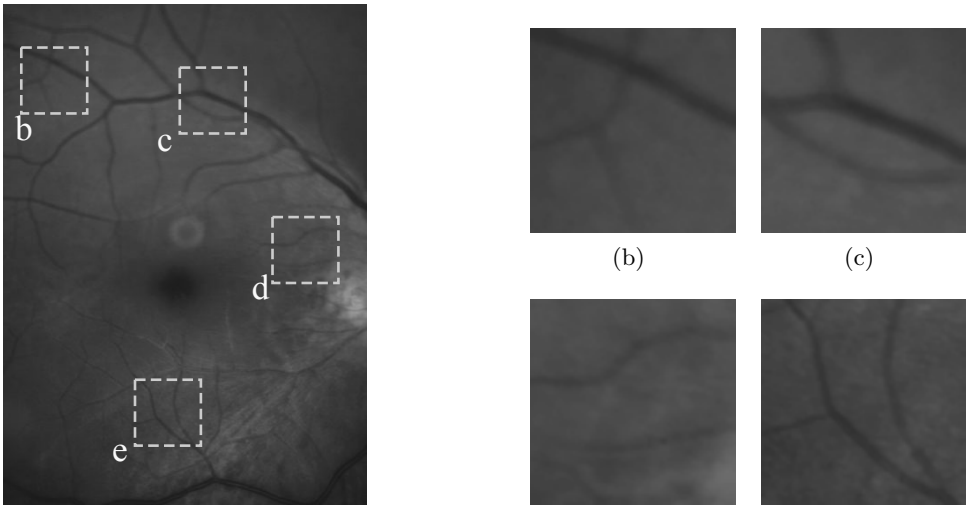

Figure 1. (a) Real case of a retinal image naturally degraded with space-variant blur caused by strong astigmatism. (b), (c), (d), and (e) zoomed regions to show the space-variant nature of the blur.

in such a way that many common eye related conditions, such as astigmatism, keratoconus, corneal refractive surgery, or even tear break-up, may contribute significantly to a decline in image quality[6,7] typically in the form of a SV degradation.

Restoration of images with SV blur from optical aberrations has been reported in the literature,[8] with the main limitation that the blurred image is often restored in regions or patches, which are then stitched together. This inevitably leads to *ringing* artifacts in transition areas. Another clear disadvantage is a marked difficulty in accurately estimating the SV PSF, for instance Bardsley et al.[9] use a phase-diversity based scheme to obtain the PSF associated with an image patch. This type of approach is common in atmospheric optics where the conditions and set-up of the imaging apparatus (typically a telescope) are well known and calibrated. Unfortunately, this is not immediately applicable to retinal imaging, at least non-adaptive optics retinal imaging. Recently, there have been several works[10–12] that try to solve the SV blind deconvolution problem from a single image. The common ground in these works is that the authors assume that the blur is only due to camera motion. They do this in order to reduce the space in which to search for SV blurs. Despite their approach being more general, the strong assumption of camera motion is simply too restrictive to be applied in retinal imaging.

2. SPACE-VARIANT MODEL OF IMAGE BLUR

In reality we know that the PSF is indeed spatially variant,[5] to such extent that in some cases the space-invariant approach completely fails, bringing forth the need for a SV approach. To address this limitation we model the blurred retinal image z as

$$z = Hu + n \ , \tag{1}$$

where the operator H is given by

$$[Hu](x,y) = \int u(s,t)h(x-s, y-t, s, t)\, dsdt \ , \tag{2}$$

u is the unblurred retinal image, h is the SV PSF, and n is zero-mean Gaussian noise. The operator H is a generalization of standard convolution where h is now a function of four variables. We can think of this operation as a convolution with a PSF that is now dependent on the position (s,t) in the image. Standard convolution is a special case of Eq. (2), where $h(x-s, y-t, s, t) = h(x-s, y-t)$ for an arbitrary position (s,t). Note that (2) is a general construct that can represent most other complex image degradations which depend on spatial coordinates, such as motion blur, optical aberrations, lens distortions and out-of-focus blur.

3. METHOD

3.1 Preprocessing

Because we use a multi-channel scheme for the estimation of the local PSFs, we assume that at least two images with similar content (field of view) are available. The images are preprocessed so that they meet the requirements imposed by the space-invariant convolutional model given by Eq. (3). This consists in registering the images and adjusting their illumination distribution following the work by Marrugo et al.[3] By carrying out this procedure the remaining radiometric differences between the images are assumed to be caused by blur and noise. Since image g is registered and its illumination matched to z, we denote this transformed auxiliary image as $\tilde{g}$.

3.2 Blind estimation of PSFs

We approximate the global function h from Eq. (2) by interpolating local PSFs estimated on a set of discrete positions. The main advantage of this approach is that the global PSF needs not be computed on a per-pixel basis which is inherently time-consuming. The procedure for estimating the local PSFs is the following. We divide the images z and $\tilde{g}$ into a grid of $m \times m$ patches. In each patch p we assume a convolutional blurring model, like in Ref. 3, where an ideal sharp patch u_p originates from two degraded patches z_p and $\tilde{g}_p$ (for $p = 1 \dots m \times m$). The local blurring model is

$$\begin{aligned} z_p &= h_p * u_p + n \\ \tilde{g}_p &= \tilde{h}_p * u_p + \tilde{n} \ , \end{aligned} \tag{3}$$

where $*$ is the standard convolution, and h_p and $\tilde{h}_p$ are the convolution kernels or local PSFs, and the noise (n and $\tilde{n}$) is assumed to be Gaussian additive with zero mean.

From this model we can estimate the local PSFs with an alternating minimization procedure as described in Ref. 3 but applied locally. We do so on a grid of 5–by–5 image patches to compute 25 PSFs, as shown in Fig. 2. The general guideline is that the patch size should be large enough to include retinal structures and much larger than the size of the local PSF. The ground-truth SV PSF grid was built from a grid of 3×3 realistic PSFs obtained from degraded retinal images using the method of Ref. 3 and interpolated to form a 5×5 grid. By visually comparing the ground-truth PSF grid with the estimated grid it is important to note that not all local PSFs have been correctly estimated. There are a number of non-valid PSFs which need to be indentified and left out from the restoration procedure to avoid artifacts.

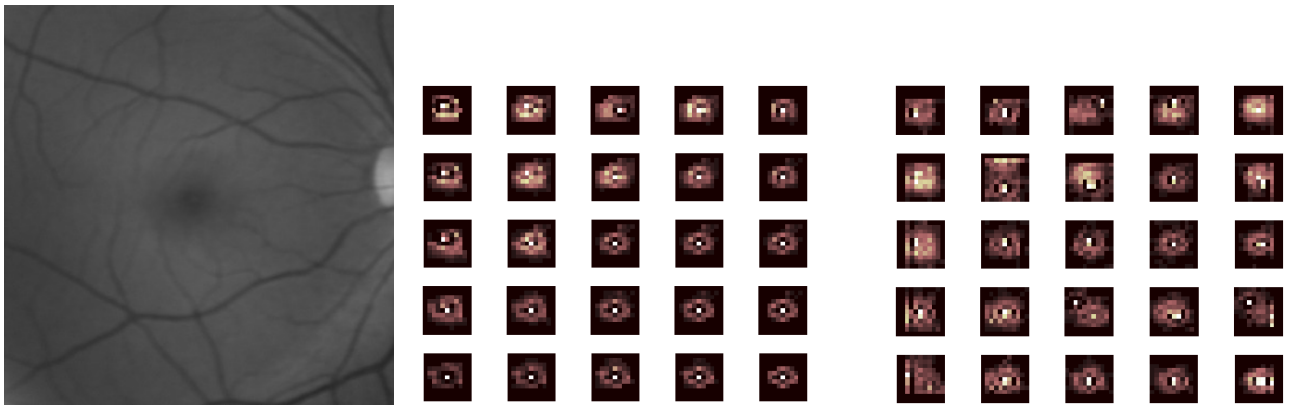

(a) (b) (c)

Figure 2. (a) Retinal image artificially degraded with SV blur. (b) Ground-truth SV PSF grid. (c) Estimated SV PSF grid.

3.3 Identification of valid local PSFs

Because reconstruction artifacts arise from poorly estimated local PSFs we have carried out artificial experiments to determine an adequate approach for identifying non-valid PSFs. Recently Hu and Yang[13] studied the problem of identifying good regions for estimating the PSF of an image degraded by motion blur. Their reasoning comes from the fact that for estimating the PSF from an image with motion blur, not all parts of the image contribute equally. Moreover, there are parts of the image that hinder the estimation procedure. In light of this, we have carried out experiments to determine if the non-valid PSFs can be identified either from the degraded retinal image or directly from the estimated PSFs. These experiments consist in artificially degrading pairs of retinal images, estimating the PSFs per patch, comparing the estimated PSFs with the original PSFs with a similarity measure, computing an image or PSF descriptor to determine an identification criterion.

3.3.1 Similarity measure

To avoid the problem with shift ambiguity of blind deconvolution, the comparison of estimated $\hat{h}_p$ and corresponding ground-truth PSF h_p is carried out by the similarity measure

$$S(h_p, \hat{h}_p) = \max_{\gamma} \rho(h_p, \hat{h}_p, \gamma) \tag{4}$$

proposed by Hu and Yang.[13] The measure is defined as the maximum response of the normalized cross correlation

$$\rho(h_p, \hat{h}_p, \gamma) = \frac{\sum_{\tau} h_p(\tau) \cdot \hat{h}_p(\tau + \gamma)}{\|h_p\| \cdot \|\hat{h}_p\|} \ , \tag{5}$$

where γ is the possible shift between the two kernels, τ represents image coordinates and $\|\cdot\|$ is the l_2 norm. Larger similarity values reflect more accurate PSF estimation.

3.3.2 The good regions approach

As we have seen in Fig. 2 the estimation of PSFs may fail and one way to avoid this is to determine suitable regions where to compute the PSFs from. In the work by Hu and Yang[13] they use low level image descriptors that focus on sharp edges or textured regions. We compute on a per-patch basis the image entropy, the sum of absolute value of the gradient in the vertical and horizontal directions, and the relative value of the patch dominant orientation based on filtering with Kirsch's templates[14] widely used for detecting the blood vessels in retinal images.[15] We also compute the sum of pixels detected as blood vessels per patch.

We compute the correlation of the similarity measure for the estimated PSFs with these image descriptors. The results are shown in Table 1. Note that not a single descriptor correlates well with similarity measure, because they do not even reach a value above 0.5 in absolute value. This approach is along the lines of Ref. 13, but it significantly differs in that we consider blur that, due to the imaging procedure, is much more complex than simple shift because of the aberrations in the eye. The work in Ref. 13 is limited to motion blur which typically produces a type of degradation that is dependent on the trajectory of motion.

3.3.3 The valid PSFs

Having found no significant correlation with the image patches we address the problem of valid PSF identification from the PSFs themselves. Because the optics of the eye is part of the imaging system, our assumption is that valid PSFs may display a shape and energy distribution that make them differentiable from PSFs where the estimation failed. In fact, the PSF typically looks as a set of concentric rings or waves. This can be detected for example by Hu rotation invariants.[16]

Indeed, from the plot we can confirm the correlation, but more importantly we can observe that most non-valid PSFs, which we assume to be the ones with $S < 0.6$, can be clearly identified. Roughly, the greater the I_4 value the lower the similarity measure. We select a threshold to remove almost all non-valid PSFs even at the expense of several valid PSFs. In Fig. 3 we show the PSFs selected as valid ones for carrying out the restoration. However, the fact that we leave out several valid PSFs is not critical because according to our model the PSF changes smoothly and having few PSFs distributed throughout the FOV should be sufficient for an accurate restoration. In the following section we demonstrate how to restore the degraded image with a SV PSF defined on irregularly distributed points of the image.

	Descriptor	Correlation coefficient
Image patch	Entropy	-0.059
	Sum of gradients	-0.187
	Dominant orientation	0.064
	Blood vessel detection	-0.044
PSF	First image moment I_1	-0.519
	Second Hu invariant I_2	-0.569
	Third Hu invariant I_3	-0.536
	Fourth Hu invariant I_4	-0.577
	Fith Hu invariant I_5	-0.082
	Sixth Hu invariant I_6	-0.394
	Seventh Hu invariant I_7	0.241

Table 1. Correlation of image patch and PSF descriptors with PSF similarity measure (S). Higher correlation coefficient in magnitude is better, it means that the descriptor is better suited for identifying valid or non-valid PSFs.

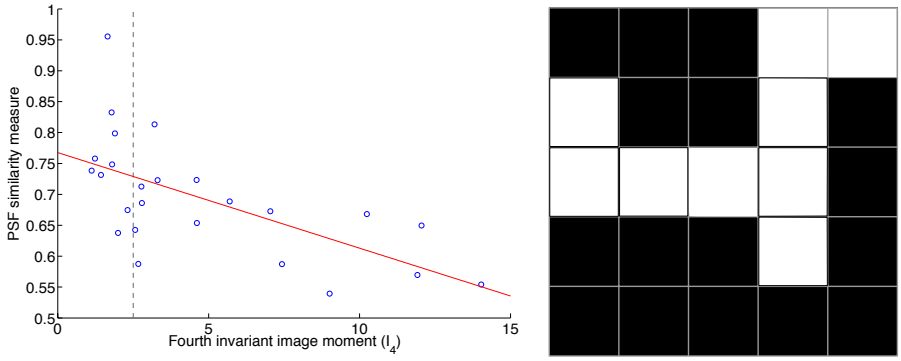

(a) (b)

Figure 3. (a) PSF similarity measure (S) versus fourth image invariant (I_4). A threshold (dashed vertical line) is selected so that most non-valid PSFs (similarity of < 0.6) are excluded from the restoration procedure. (b) The PSFs selected as valid ones (white squares) for carrying out the restoration.

3.4 PSF interpolation and image restoration

Having determined the valid PSFs we address the problem of computing a space-variant PSF for restoring the whole image. We compute the Delaunay triangulation on the positions of the PSFs and perform linear interpolation within each triangle with interpolation coefficents given by barycentric coordinates. This defines a continuous SV PSF for irregularly distributed valid PSFs. The restoration can be described as the minimization of the functional

$$\min_u \left[\frac{1}{2} \|z - Hu\|^2 + \lambda \int |\nabla u| \, dxdy \right] \quad , \tag{6}$$

where z is the blurred observed image, H is the blurring operator (Eq. (2)), u is the unknown sharp image, and λ is a positive regularization constant, which we have set according to a fine-tuning procedure.[3] The first term penalizes the discrepancy between the model and the observed image. The second term is the regularization term which serves as a statistical prior. As regularization we use total variation, a technique that exploits the sparsity of image gradients in natural images. At present, solving the convex functional of Eq. (6) is considered a standard way to achieve close to state-of-the-art restoration quality without excessive time requirements.[17] We used an efficient method[18] to solve Eq. (6) iteratively as a sequence of quadratic functionals

$$u_{i+1} = \arg\min_u \left[\frac{1}{2} \|z - Hu\|^2 + \lambda \int \frac{|\nabla u|^2}{2|\nabla u_i|} + \frac{|\nabla u_i|}{2} \, dxdy \right] \quad . \tag{7}$$

Eq. (7) bounds the original function in Eq. (6) and has the same value and gradient in the current u_i, which guarantees convergence to the global minimum. To solve Eq. (7) we used the conjugate gradient method.[19]

4. EXPERIMENTS AND RESULTS

To demonstrated the applicability of the proposed method we have designed several experiments on both artificial and real degraded retinal images. The artificial experiment was devised mainly for validating the proposed method.

4.1 Artificially Degraded Images

For the artificial experiment we take a pair of images and degrade them with a 5×5 grid of realistic PSFs plus Gaussian noise ($\sigma = 10^{-6}$). The grid of PSFs was built upon estimated PSFs from retinal images following the approach of Ref. 3. We restore a single image, the second image is used exclusively for the purpose of PSF estimation. We estimate the local PSFs by dividing the image into overlapping patches on a 5×5 grid. The estimated PSFs are shown in Fig. 2. Because the PSF estimation may fail, we identify the valid PSFs as described in § 3.3. Using the positions of valid PSFs we construct the Delaunay triangulation and perform linear interpolation of the PSFs to obtain the SV PSF for the whole image.

In Fig. 2(a) we show the restored artificial image with the direct estimated PSFs. The effect of non-valid PSFs is evident in the poor quality of the restoration and the ringing artifacts. In Fig. 2(b) we show the restoration with the proposed method. To evaluate the restoration we use the cumulative error histogram on a patch basis. The error[4] is the difference between a recovered image I_r with the estimated kernels and the known ground-truth sharp image I_g over the difference between the deblurred image I_{kg} with the ground-truth kernels. The error is given by $\|I_r - I_g\|/\|I_{kg} - I_g\|$. In Fig. 4(c) we show the cumulative error histogram for three restorations. H1 is the restoration with the directly estimated PSFs. It is important to note that shifted local PSFs warp the image which introduce additional artifacts and is the reason for such low performance with approximately 40% of patches with an error lower than 2.5. After shifting the centroid of the PSFs to the geometrical center (restoration H2 in Fig. 4(c)) the reconstruction error is reduced significantly, about 60% of patches have an error lower than 1.5. Finally, the restoration (H3) with the valid PSFs increases significantly with all patches now displaying an error lower than 1.5.

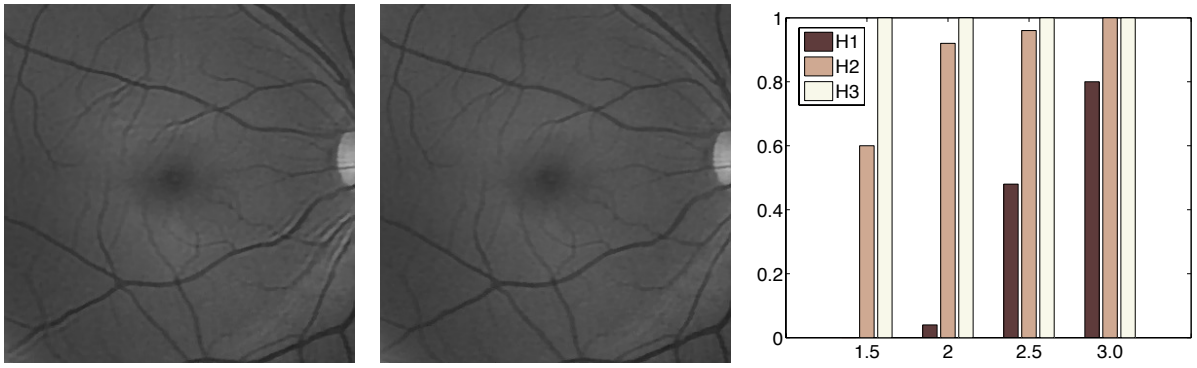

(a) (b) (c)

Figure 4. (a) Restoration with direct estimated PSFs (notice the artifacts due to non-valid PSFs) and (b) proposed interpolation of valid PSFs. (c) Error histogram for evaluating the reconstruction using: H1-directily estimated PSFs, H2-PSFs shifted toward the geometrical center, and H3-the valid PSFs interpolated over the whole image.

4.2 Naturally Degraded Images

As we illustrated in Fig. 1 there are a number of conditions that lead to space-variant degradations of retinal images, for example strong astigmatism. In Fig. 5 we show the real case of an original degraded retinal image alongside the SV restoration with the directly estimated local PSFs and proposed SV restoration with the PSFs selected by the strategy defined in § 3.3.3. Notice how the image in Fig. 5(b) has artifacts originated from poorly

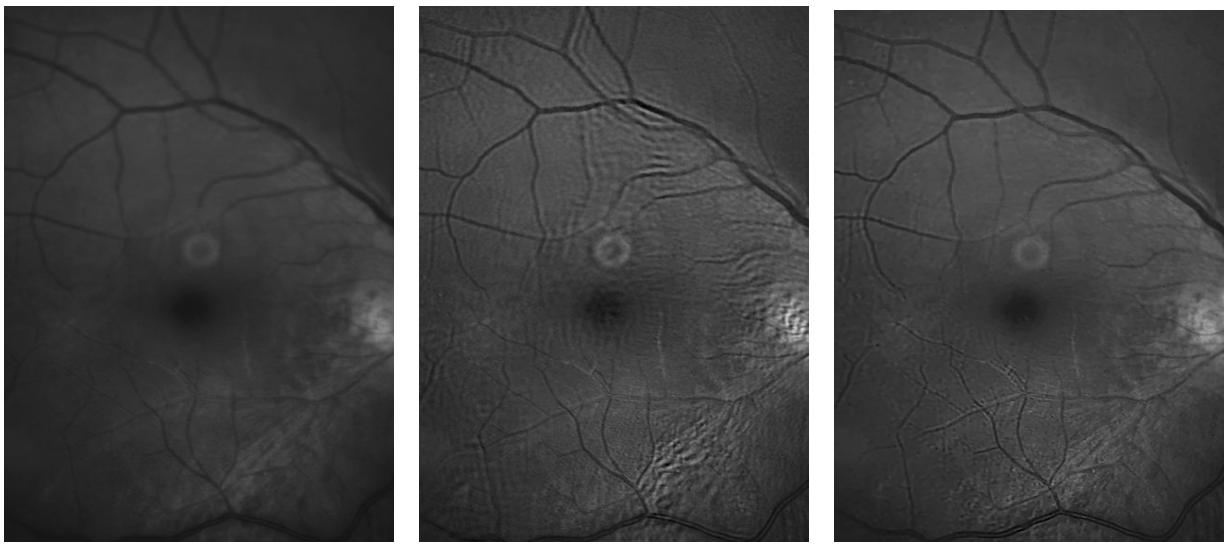

(a) (b) (c)

Figure 5. (a) Original degraded image from Fig. 1(a), (b) space-variant restoration with direct estimated PSFs, and (c) space-variant restoration with linear interpolation of valid PSFs.

estimated PSFs. In contrast, the image in Fig. 5(c) is much sharper with with fine structures like blood vessels more properly resolved. In Fig 6 we show the grid of estimated PSFs and the valid PSFs selected with the strategy defined in § 3.3.3 highlighted with red squares.

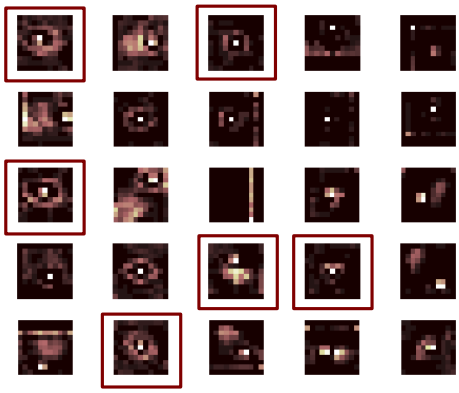

Figure 6. PSF grid estimated for the real degraded retinal image from Fig. 1(a). The PSFs within red squares correspond to the valid PSFs selected according to the criterion described in § 3.3.3.

5. CONCLUSION

We have presented a method for restoring retinal images degraded with space-variant blur. The space-variant PSF is approximated via the interpolation of local space-invariant PSFs estimated from a pair of degraded retinal images. Because the PSF estimation may fail we developed a PSF selection strategy based on image invariant moments to identify valid PSFs. To perform the restoration we interpolated the valid PSFs based on the Delaunay triangulation with vertices defined on an arbitrary point of the image. With the artificial experiment we showed how our approach significantly reduces the reconstruction error, being less prone to artifacts. The results on naturally degraded images validate our apporach with notable enhancement throughout the whole image.

ACKNOWLEDGMENT

This research has been partly funded by the Spanish Ministerio de Ciencia e Innovación y Fondos FEDER (project DPI2009-08879) and projects TEC2010-09834-E and TEC2010-20307. Financial support was also provided by the Grant Agency of the Czech Republic under project 13-29225S. The first author also thanks the Spanish Ministerio de Educación for an FPU doctoral scholarship.

REFERENCES

[1] Godara, P., Dubis, A. M., Roorda, A., Duncan, J. L., and Carroll, J., "Adaptive optics retinal imaging: emerging clinical applications," *Optometry and vision science : official publication of the American Academy of Optometry* **87**, 930–941 (Dec. 2010).

[2] Arines, J. and Acosta, E., "Low-cost adaptive astigmatism compensator for improvement of eye fundus camera," *Optics Letters* **36**, 4164–4166 (Nov. 2011).

[3] Marrugo, A. G., Sorel, M., Sroubek, F., and Millán, M. S., "Retinal image restoration by means of blind deconvolution," *Journal of Biomedical Optics* **16**(11), 116016 (2011).

[4] Levin, A., Weiss, Y., Durand, F., and Freeman, W., "Understanding Blind Deconvolution Algorithms," *Pattern Analysis and Machine Intelligence, IEEE Transactions on* **33**(12), 2354–2367 (2011).

[5] Bedggood, P., Daaboul, M., Ashman, R., Smith, G., and Metha, A., "Characteristics of the human isoplanatic patch and implications for adaptive optics retinal imaging," *Journal of Biomedical Optics* **13**(2), 024008 (2008).

[6] Tutt, R., Bradley, A., Begley, C., and Thibos, L. N., "Optical and visual impact of tear break-up in human eyes," *Investigative Ophthalmology & Visual Science* **41**, 4117–4123 (Dec. 2000).

[7] Xu, J., Bao, J., Deng, J., Lu, F., and He, J. C., "Dynamic Changes in Ocular Zernike Aberrations and Tear Menisci Measured with a Wavefront Sensor and an Anterior Segment OCT," *Investigative Ophthalmology & Visual Science* **52**, 6050–6056 (July 2011).

[8] Costello, T. and Mikhael, W., "Efficient restoration of space-variant blurs from physical optics by sectioning with modified Wiener filtering," *Digital Signal Processing* **13**(1), 1–22 (2003).

[9] Bardsley, J., Jefferies, S., Nagy, J., and Plemmons, R., "A computational method for the restoration of images with an unknown, spatially-varying blur.," *Optics express* **14**, 1767–1782 (Mar. 2006).

[10] Harmeling, S., Hirsch, M., and Scholkopf, B., "Space-variant single-image blind deconvolution for removing camera shake," *Advances in Neural Inform. Processing Syst* (2010).

[11] Whyte, O., Sivic, J., Zisserman, A., Ponce, J. C. V., and on, P. R. C. . I. C., "Non-uniform deblurring for shaken images," in [*Computer Vision and Pattern Recognition (CVPR), 2010 IEEE Conference on*], 491–498 (2010).

[12] Gupta, A., Joshi, N., Lawrence Zitnick, C., Cohen, M., and Curless, B., "Single image deblurring using motion density functions," *Computer Vision–ECCV 2010* , 171–184 (2010).

[13] Hu, Z. and Yang, M.-H., "Good regions to deblur," in [*Computer Vision–ECCV 2012*], 59–72, Springer (2012).

[14] Kirsch, R. A., "Computer determination of the constituent structure of biological images," *Computers and biomedical research* **4**(3), 315–328 (1971).

[15] Al-Rawi, M., Qutaishat, M., and Arrar, M., "An improved matched filter for blood vessel detection of digital retinal images," *Computers in Biology and Medicine* **37**(2), 262–267 (2007).

[16] Hu, M.-K., "Visual pattern recognition by moment invariants," *Information Theory, IRE Transactions on* **8**(2), 179–187 (1962).

[17] Campisi, P. and Egiazarian, K., [*Blind image deconvolution: theory and applications*], CRC Press, Boca Raton, Fl, USA (2007).

[18] Chambolle, A. and Lions, P. L., "Image recovery via total variation minimization and related problems," *Numerische Mathematik* **76**(2), 167–188 (1997).

[19] Golub, G. and Van Loan, C., [*Matrix computations*], vol. 3, Johns Hopkins University Press (1996).